

# Non-Hermitian $\mathbb{Z}_2$ Photonic Topological Insulators

Rodrigo P. Câmara,<sup>1</sup> Tatiana G. Rappoport,<sup>1,2</sup> and Mário G. Silveirinha<sup>1</sup>

<sup>1</sup>*Instituto Superior Técnico and Instituto de Telecomunicações,  
University of Lisbon, Avenida Rovisco Pais 1, Lisboa, 1049001 Portugal*

<sup>2</sup>*Instituto de Física, Universidade Federal do Rio de Janeiro,  
C.P. 68528, 21941-972 Rio de Janeiro RJ, Brazil*

(Dated: February 1, 2023)

Photonic platforms invariant under the action of parity, time-reversal, and duality ( $\mathcal{P} \cdot \mathcal{T} \cdot \mathcal{D}$ ) operators may host topological phases that are the counterpart of those supported by time-reversal invariant  $\mathbb{Z}_2$  electronic systems. Here, we uncover the robustness of the  $\mathbb{Z}_2$  photonic phases to non-Hermitian effects, e.g., to material dissipation. In particular, it is shown that non-Hermitian  $\mathcal{PD}$  reciprocal photonic insulators may be split into two classes of topologically inequivalent materials, whose interfaces may support spin-polarized states. To illustrate our theory, we study in detail how the non-Hermitian effects may sculpt the topology of a  $\mathcal{PD}$  symmetric parallel-plate waveguide (PPW). We find that there is a critical level for the plates loss that separates two different topological phases. We identify the phases by their spin Chern numbers and analyze the transition.

Topological photonics<sup>1,2</sup> determines a rather unique paradigm to create unidirectional channels immune to back-scattering. The topological protection of Chern insulators originates from an electromagnetic “quantum Hall effect” rooted in the time-reversal symmetry breaking<sup>3,4</sup>. In analogy with the quantum spin Hall effect in electronic systems<sup>5</sup>, time-reversal invariant photonic structures may also host topological phases<sup>6–16</sup>. However, due to the different nature of fermionic and bosonic particles, additional symmetries must be enforced on a system to guarantee the  $\mathbb{Z}_2$  topological protection, most notably a duality symmetry that ensures balanced electric and magnetic responses<sup>10</sup>.

To our best knowledge, the most general symmetry transformation that enables the  $\mathbb{Z}_2$  topological protection in photonic systems is determined by a combination of the parity ( $\mathcal{P}$ ), time-reversal ( $\mathcal{T}$ ) and duality ( $\mathcal{D}$ ) operators,  $\tilde{\mathcal{T}} = \mathcal{PTD}$ <sup>10,17–19</sup>. The  $\tilde{\mathcal{T}}$  operator may be regarded as a pseudo-time-reversal operator, as it is anti-linear and satisfies  $\tilde{\mathcal{T}}^2 = -\mathbf{1}$ . Such a property guarantees that the photonic states of a  $\mathcal{PTD}$ -symmetric system are degenerate (Kramers theorem)<sup>10,17</sup> and that there is a suitable basis in which the scattering matrix is anti-symmetric<sup>17</sup>. The latter property implies that when a  $\mathcal{PTD}$ -symmetric system supports an odd number of bi-directional channels, it is feasible to have bi-directional transport of light without any back-reflections<sup>17</sup>.

Previous studies on  $\mathcal{PTD}$ -symmetric systems dealt exclusively with energy conserving (Hermitian) platforms. The study of topological phases was recently extended to non-Hermitian systems through a generalization of the notion of band gaps to complex spectra<sup>20,21</sup>. As a result, topological properties with no counterpart in nonreciprocal<sup>3,4,22–27</sup> and time-reversal invariant<sup>6–15</sup> closed systems have been found<sup>21,28,28–38</sup>. Exceptional points (parameter space points where energies and associated modes coalesce simultaneously)<sup>39–43</sup> are linked to exotic effects<sup>44–50</sup> and unprecedented phases of matter<sup>21,31–38</sup>.

Here, we study the impact of non-Hermitian effects,

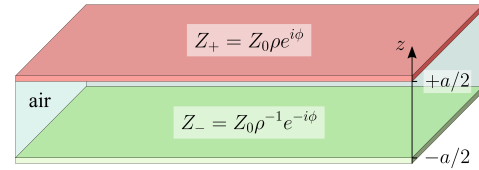


Figure 1: Structure of the  $\mathcal{PD}$ -symmetric parallel-plate waveguide with a dielectric block (air) of width  $a$  in between two impedance surfaces.

notably material dissipation, on the topological phases of  $\mathcal{PTD}$  symmetric systems. We find that the  $\mathbb{Z}_2$  topological index is highly robust to the presence of material absorption, and most interestingly we identify a topological phase transition controlled by the loss parameter strength.

Amongst the different  $\mathbb{Z}_2$  photonic topological insulators considered in previous works<sup>18,19,51–53</sup>, we are interested in a generalization of a structure introduced in Ref. 18. It is a parallel-plate waveguide (PPW) [see Fig. 1] with the electromagnetic response of the top and bottom plates linked by electromagnetic duality. Each plate is modeled through an impedance (Leontovitch) boundary condition such that  $Z_i \hat{\mathbf{n}} \times \mathbf{H} = \mathbf{E}_{\text{tan}}$  with  $\hat{\mathbf{n}}$  the unit normal vector to the plate (directed towards the dielectric),  $\mathbf{E}_{\text{tan}} = \mathbf{E} - \hat{\mathbf{n}}(\hat{\mathbf{n}} \cdot \mathbf{E})$  is tangential electric field, and  $Z_i$  is the surface impedance of the  $i = +, -$  (top/bottom, respectively) plate. In order that the system is parity-duality  $\mathcal{PD}$  symmetric it is necessary that  $Z_+ Z_- = Z_0^2$  with  $Z_0$  the vacuum impedance. Similar to Ref. 17, we define the parity transformation such that  $(x, y, z) \rightarrow (x, y, -z)$  and the duality transformation such that  $\mathcal{D} : (\mathbf{E}, \mathbf{H}) \rightarrow (\mathbf{H} Z_0, -\mathbf{E}/Z_0)$  [see Supplementary Material 54]. The parity transformation exchanges the position of the two plates, whereas the duality mapping transforms  $Z_+ \rightarrow Z_-$  and vice-versa. Thus, the  $\mathcal{PD}$  transformation leaves the system invariant when the region in between the plates is filled with air. The condition  $Z_+ Z_- = Z_0^2$  implies that the impedances of the plates are

of the type  $Z_+ = Z_0 \rho e^{i\phi}$  and  $Z_- = Z_0 \rho^{-1} e^{-i\phi}$ , with  $\rho$  and  $\phi$  dimensionless parameters. Thus, when the top plate has an inductive response ( $\phi < 0$ , for a time variation  $e^{-i\omega t}$ ) then the bottom plate has a capacitive response  $\phi > 0$ , and vice-versa. In the limit  $\rho \rightarrow 0$  the top (bottom) plate behaves as a perfect electric (magnetic) conductor, i.e., a PEC (PMC). For simplicity, to avoid complications related to material dispersion, in this Letter we shall suppose that the surface impedances  $Z_{\pm}$  are real-valued ( $\phi = 0$ ) and frequency independent. Then, for  $0 < \rho < \infty$  the waveguide is non-Hermitian as both the top and bottom plates absorb the fields propagating in the dielectric. The system is time-reversal invariant (and  $\mathcal{PTD}$ -symmetric) only when  $\rho = 0$ , i.e., for PEC and PMC walls. For generality, we shall also consider the case of a negative resistivity,  $\rho < 0$ , which models the case of “gainy” (active) plates. Even though the propagation of spin-polarized edge modes in related guides was discussed in different works<sup>18,55</sup>, this type of system still lacks of an appropriate topological classification, even in the Hermitian case.

For  $\mathcal{PD}$  symmetric *reciprocal* systems, such that  $\varepsilon(x, y, z) = \mu(x, y, -z)$ , the frequency-domain (source-free) Maxwell equations can be split into two independent sets of equations<sup>18</sup>

$$\pm \frac{ic}{\varepsilon(z)} \begin{pmatrix} 0 & \partial_z & \partial_y \\ -\partial_z & 0 & -\partial_x \\ \partial_y & -\partial_x & 0 \end{pmatrix} \Psi^{\pm}(-z) = \omega \Psi^{\pm}(z), \quad (1)$$

that are formally equivalent to  $\hat{\mathcal{H}}^{\pm} \Psi^{\pm}(z) \equiv \omega \Psi^{\pm}(z)$  with the pseudospinors  $\Psi^{\pm}$  written in terms of the electric and magnetic fields  $\mathbf{E}$  and  $\mathbf{H}$  as  $\Psi^{\pm}(z) = (E_x(z) \mp Z_0 H_x(-z), E_y(z) \mp Z_0 H_y(-z), E_z(z) \pm Z_0 H_z(-z))^T$ <sup>18</sup>. Here,  $c$  denotes the speed of light in vacuum and  $\omega$  is the oscillation frequency. For conciseness we denote a generic point of space  $(x, y, z)$  as  $(z)$ , and the mirror-symmetric point  $(x, y, -z)$  as  $(-z)$ . As  $\mathbf{E} = \frac{1}{2}(\Psi^+ + \Psi^-)$ , the dynamics of a generic electric field distribution is fully controlled by the dynamics of the two pseudospinors [Eq. (1)]. Notably, different from the original Maxwell’s equations the dynamics of the pseudo-spinors is strongly nonlocal, as the two sides of Eq. (1) are evaluated at mirror-symmetric points. Interestingly, the pseudospinor decomposition holds true even when the dielectric response is lossy (e.g., if  $\varepsilon$  is frequency dependent and complex-valued) or when the plate walls have a non-Hermitian response.

In the Hermitian case, when the dielectric and the plates are lossless, the class of eigenstates with pseudospin “+” can be transformed into eigenstates with pseudospin “-” using the time-reversal operator. Even though such a construction is not feasible in the non-Hermitian case, the key observation is that the electromagnetic reciprocity of the system guarantees that the total topological charge is zero<sup>20</sup>, similar to the fermionic case case<sup>56</sup>. Thereby the topological charge of the operators  $\hat{\mathcal{H}}^{\pm}$  in Eq. (1) must be exactly symmetric:  $\mathcal{C}^+ + \mathcal{C}^- = 0$ . Here,  $\mathcal{C}^{\pm}$  are the spin Chern numbers associated with a band

gap of interest. Therefore,  $\mathcal{PD}$  symmetric reciprocal systems may host nontrivial topological phases determined by the invariant  $\mathcal{C}^+ = -\mathcal{C}^-$ . In the following, we apply the non-Hermitian topological band theory to determine the topological phase diagram<sup>21</sup>.

The dielectric in Fig. 1 is taken as air ( $\varepsilon = \mu = 1$ ), so that non-Hermitian effects arise exclusively due to the plates. As the system is invariant under continuous translations in the  $xoy$  plane, the pseudospin states can be factorized as  $\Psi^{\pm}(\mathbf{r}, t) = \Psi_{\mathbf{k}}^{\pm}(z) e^{-i\omega t} e^{i\mathbf{k} \cdot \mathbf{r}}$ , where  $\mathbf{k}$  is the in-plane real-valued wave vector ( $\mathbf{k} \cdot \hat{\mathbf{z}} = 0$ ) with magnitude  $k$ . The eigenstates are found by solving the Maxwell’s equations subject to the appropriate boundary conditions in the original guide, followed by a projection onto the two pseudospinor subspaces<sup>54</sup>. As the guide is invariant under arbitrary rotations around the  $z$ -axis it is convenient to write a generic eigenstate in terms of the vectors  $(\hat{\mathbf{k}}, \hat{\mathbf{z}} \times \hat{\mathbf{k}}, \hat{\mathbf{z}})$ . The coordinates of a generic pseudospin state with eigenfrequency  $\omega_n = \omega_n(k)$  in this basis are:

$$\Psi_{\mathbf{k}, n}^{\pm}(z) \rightarrow \begin{pmatrix} \mp (e^{-i\kappa_n z} + h_n e^{i\kappa_n z}) \\ -\frac{\omega_n}{c\kappa_n} (e^{i\kappa_n z} - h_n e^{-i\kappa_n z}) \\ \frac{k}{\kappa_n} (e^{-i\kappa_n z} - h_n e^{i\kappa_n z}) \end{pmatrix} \quad (2)$$

where  $h_n \equiv e^{i\kappa_n a} \frac{\omega_n - c\rho\kappa_n}{\omega_n + c\rho\kappa_n}$ ,  $\kappa_n = \kappa_n' + i\kappa_n''$  is the transverse wavenumber, and the label  $n = 1, 2, \dots$  identifies the different modes. For each  $k$  real-valued, the allowed values for  $\kappa_n$  can be found by solving the modal condition

$$e^{2i\kappa_n a} = \frac{\omega_n + c\rho\kappa_n}{\omega_n - c\rho\kappa_n} \frac{\rho\omega_n + c\kappa_n}{\rho\omega_n - c\kappa_n}. \quad (3)$$

where  $\omega_n = \omega_n' + i\omega_n'' = s \times c\sqrt{k^2 + \kappa_n^2}$  with the square root branch determined by  $s = \pm$ . The dispersion  $\omega_n^{(+)}$  of the branches with positive frequencies ( $s = +$ ) is linked to the dispersion  $\omega_n^{(-)}$  of the branches with negative frequencies ( $s = -$ ) as  $\omega_n^{(+)} = -\omega_n^{(-)*}$ . This property is a consequence of the reality of the electromagnetic field (particle-hole symmetry). Both  $\kappa_n$  and  $\omega_n$  are functions of the in-plane momentum  $k$  and of the resistivity  $\rho$ . Moreover, one can always assume that  $\text{Re}\{\kappa_n\} > 0$ . The modal equation is independent of the pseudospin, and thereby the spectrum of the operators  $\hat{\mathcal{H}}^{\pm}$  is identical.

Albeit Eq.(3) is transcendental, its solutions for  $k = 0$  can be analytically determined as  $\kappa_n = (2n - 1)\pi/2a - s \times i\mathcal{F}(\rho)/a$ <sup>54</sup> with  $s = \pm$  as before and  $\mathcal{F}(\rho) = \text{sgn}(\rho) \ln \left| \frac{|\rho|+1}{|\rho|-1} \right|$ . The profiles  $\kappa_n(k)$  for  $k \neq 0$  are obtained from a numerical continuation of the  $k = 0$  solutions via a Nelder-Mead minimization scheme<sup>57</sup>.

Figures 2(a) and 2(b) show the real and imaginary parts of  $\kappa_n(k)$  for the first few guided modes for a system with  $\rho = 0$  (dashed lines) and  $\rho = 0.6$  (solid lines). The corresponding oscillation frequencies  $\omega_n(k)$  are depicted in Figs. 2(c) and 2(d). When the system is conservative ( $\rho = 0$ ), the modal equation (3) reduces to  $e^{2i\kappa_n a} = -1$ . Its solutions  $\kappa_n = (2n - 1)\pi/2a$  with

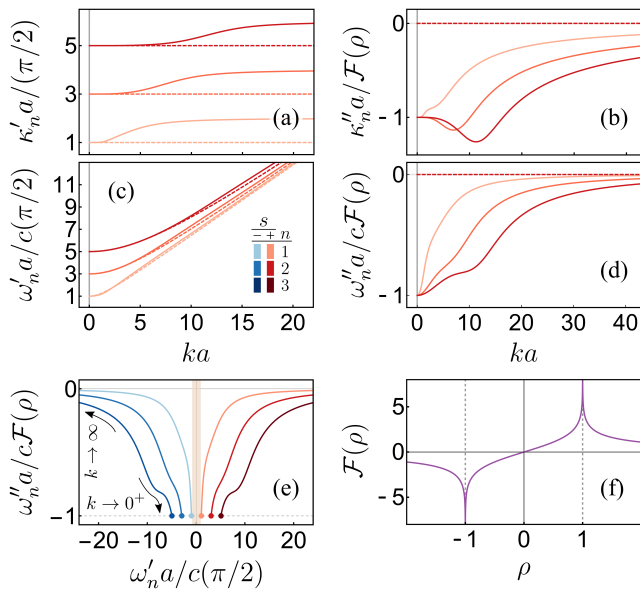


Figure 2: Dispersion diagrams for a  $\mathcal{PD}$ -symmetric waveguide with the top wall characterized by  $\rho = 0$  (dashed curves) or by  $\rho = 0.6$  (solid curves). (a) Real  $\kappa'_n$  and (b) imaginary  $\kappa''_n$  parts of the modal transverse wavenumber as functions of  $k$  for the modes with  $n = 1, 2, 3$ . (c) Real  $\omega'_n$  and (d) imaginary  $\omega''_n$  parts of the corresponding frequency bands  $\omega_n^{(\pm)}(k)$ . The imaginary parts in (b) and (d) are normalized to the function  $\mathcal{F}(\rho)$  sketched in panel (f). (e) Projected band structure in the complex plane for the case  $\rho = 0.6$ . The red and blue curves represent the positive and negative frequency branches  $\omega_n^{(+)}(k)$  and  $\omega_n^{(-)}(k)$ , respectively. The frequencies associated with  $k = 0$  are represented by the solid dots.

$n = 1, 2, \dots$  are real-valued and independent of the in-plane momentum  $k$ . Thus, as expected, the oscillation frequencies  $\omega_n^{(\pm)} = \pm c\sqrt{k^2 + \kappa_n^2}$  are real-valued in this case.

In contrast, in the dissipative (non-Hermitian) case ( $\rho = 0.6$ ), both  $\kappa_n$  and  $\omega_n$  are complex-valued. Furthermore, as seen in Fig. 2(a), for lossy plates the real part of  $\kappa_n$  acquires a positive offset of  $\pi/2a$  as  $k$  approaches infinity. In fact, when  $k \rightarrow \infty$  with  $\rho \neq 0$  the modal equation reduces to  $e^{2i\kappa_n a} = 1$  (the terms involving  $\kappa_n$  are negligible compared to the terms involving  $\omega_n$  in Eq. (3), which yields  $\kappa_n(\infty) = 2n\pi/2a$ . Moreover, in the  $k \rightarrow \infty$  limit the in-plane wavelength becomes much shorter than the plates distance  $a$ , and thereby the dispersion of the modes approaches asymptotically that of the dielectric so that  $\omega_n(k) \approx ck$  [see Figs. 2(c) and 2(d)].

The imaginary part of the complex frequency  $\omega_n$  determines the decay rate (in time) of the mode, which is a clear fingerprint of the non-Hermitian dynamics. Interestingly, the decay rate is boosted for  $\rho \sim \pm 1$ , which correspond to the singularities of the function  $\mathcal{F}(\rho)$  [see Fig. 2(f)]. Heuristically, this happens because for  $\rho \sim 1$  there is an impedance match between the plates and the dielectric region. Defining  $\delta = 1 - |\rho|$  as the offset of  $|\rho|$  from a critical point, the logarithmic nature of the singu-

larities  $\kappa_n \approx \pm ia^{-1} \ln |\delta/2|$  and  $\omega_n \approx \pm ica^{-1} \ln |\delta/2|$  is unravelled for  $|\delta| \ll 1$  with  $\rho \rightarrow \pm 1$ , at  $k = 0$ . This corresponds to a time variation of the type  $|\delta/2|^{\pm ct/a}$  so that both pseudospins are either rapidly suppressed or amplified in these resonant conditions ( $\rho = \pm 1$  for lossy/gainy walls). It is useful to note that for  $\rho = \pm 1$  the top and bottom plates are identical. In fact, replacing  $\rho$  with  $1/\rho$  is equivalent to interchange the the top and bottom plates due to the  $\mathcal{PD}$  symmetry of the system.

Figure 2(e) represents the projected band structure (locus of  $\omega_n^{(\pm)}(k)$  for all  $k$  real-valued) for  $\rho = 0.6$ . The figure shows both the positive frequency  $\omega_n^{(+)}(k)$  and negative frequency  $\omega_n^{(-)}(k)$  branches. As seen, a band gap separates the positive and negative frequency parts of the spectrum (beige rectangular region centered at  $\omega = 0$ ). Similar band structures are obtained for other values of  $\rho$ , provided  $\rho$  is not near the critical points  $\pm 1$ . The projected band structure lies in the lower-half (upper-half) frequency plane for  $\rho > 0$  ( $\rho < 0$ ), i.e., for lossy (gainy) plates. Furthermore, due to the particle-hole symmetry ( $\omega_n^{(+)} = -\omega_n^{(-)*}$ ) there is a mirror symmetry about the imaginary frequency axis. Typically, different branches of the projected band structure are disjoint and there are no intersections (or self-intersections). However, as further discussed below, for  $\rho \sim \pm 1$  the band gap centered about the imaginary axis can close and the different branches can exchange topological charge.

The topological classification of a generic non-Hermitian operator  $\hat{\mathcal{H}} \neq \hat{\mathcal{H}}^\dagger$  requires considering a biorthogonal basis of left  $\phi_n^L$  and right  $\phi_n^R$  eigenstates such that  $\hat{\mathcal{H}}^\dagger \phi_n^L = E_n^* \phi_n^L$  and  $\hat{\mathcal{H}} \phi_n^R = E_n \phi_n^R$ , with  $E_n$  the eigenvalues of  $\hat{\mathcal{H}}$ . The left and right eigenstates are normalized as  $\langle \phi_n^L | \phi_m^R \rangle = \delta_{nm}$ . In our system, switching loss into gain is equivalent to switch the sign of  $\rho$ . Thus, the operator  $\hat{\mathcal{H}}^\dagger$  models a PPW with resistivity  $-\rho$ . This means that  $\Psi_n^L(z; \rho) = \Psi_n^R(z; -\rho)$ . The eigenfunctions of the adjoint operator can then be obtained from Eq. (2) using the rule  $\rho \rightarrow -\rho$  (the same rule is applied to the dispersion equation (3); in particular, we have  $\omega_n(-\rho) = \omega_n^*(\rho)$  and  $\kappa_n(-\rho) = \kappa_n^*(\rho)$ ).

We use the non-Hermitian topological band theory<sup>21</sup> to determine the Chern numbers  $\mathcal{C}_n^\pm$  associated with the photonic branches of the operator  $\hat{\mathcal{H}}^\pm$ . As previously noted, for  $\rho$  not too close from the the singularities  $\pm 1$  the branches are well separated and hence their individual topological charge is well defined. We introduce the Berry potential  $\mathcal{A}_{\mathbf{k},n}^\pm = i \langle \Psi_{\mathbf{k},n}^\pm(-\rho) | \nabla_{\mathbf{k}} \Psi_{\mathbf{k},n}^\pm(\rho) \rangle$  constructed from normalized versions  $\Psi_{\mathbf{k},n}^\pm$  of the pseudospinors in Eq.(2) satisfying  $\langle \Psi_{\mathbf{k},n}^\pm(-\rho) | \Psi_{\mathbf{k},n}^\pm(\rho) \rangle = 1$ <sup>21</sup>. The inner product of two vectors  $\mathbf{F}$  and  $\mathbf{Q}$  is defined as  $\langle \mathbf{F}(z) | \mathbf{Q}(z) \rangle = \int_{-a/2}^{a/2} dz \mathbf{F}^\dagger(z) \cdot \mathbf{Q}(z)$ . In our system, the wave vector  $\mathbf{k}$  is unbounded in the Euclidean plane but the latter may be compactified into the Riemann sphere, following Ref.<sup>58</sup>. The topology is thus well-defined because the eigenfunctions in Eq.(2) are either real-valued or pure-imaginary in the limit  $k = \infty$ ,

rendering  $\mathcal{A}_{\mathbf{k},n}^\pm$  null in that gauge. In other words, the Hamiltonian  $\hat{\mathcal{H}}^\pm$  is well-behaved at  $k = \infty$ <sup>58</sup>. For the same gauge, the Berry potential is smooth in the entire momentum space, except possibly at  $k = 0$ . Then, applying the Stokes' theorem one sees that the Chern number of the  $n$ -th branch is given by  $\mathcal{C}_n^\pm = (2\pi)^{-1} [\lim_{k \rightarrow \infty} - \lim_{k \rightarrow 0^+}] k \int_0^{2\pi} d\phi \mathcal{A}_{\mathbf{k},n}^\pm \cdot \hat{\phi}$ <sup>58</sup>. Here,  $(k, \phi) \in [0, \infty[ \times [0, 2\pi[$  determine a system of polar coordinates in the  $\mathbf{k}$ -space. The azimuthal component of the Berry potential  $\mathcal{A}_{\phi,n}^\pm = \mathcal{A}_{\mathbf{k},n}^\pm \cdot \hat{\phi}$  is independent of the orientation of the wave vector  $\mathbf{k}$ , as the waveguide is unchanged under arbitrary rotations about the  $z$ -axis. Taking into account that  $\mathcal{A}_{\mathbf{k},n}^\pm$  vanishes at infinity, we conclude that  $\mathcal{C}_n^\pm = -\lim_{k \rightarrow 0^+} k \mathcal{A}_{\phi,n}^\pm(k)$ . A detailed calculation shows that<sup>54</sup>

$$\mathcal{C}_n^+ = s \times (-1)^{n+1} \text{sgn}(\delta) \quad \text{with} \quad \delta = 1 - |\rho|, \quad (4)$$

where the  $s = \pm$  sign is determined by the frequency branch ( $\omega_n^{(s=\pm)}$ ). As previously noted, due to reciprocity  $\mathcal{C}_n^- = -\mathcal{C}_n^+$ . Remarkably, the different topological phases are separated by the critical values  $\rho = \pm 1$ .

Figures 3(a) and 3(b) illustrate how higher-order photonic branches ( $n = 2, 3, \dots$ ) remain disconnected in the vicinity of  $\rho = 1$ . They also hint the divergences  $\omega_n'' \rightarrow -\infty$  at  $k = 0$  and  $\rho = 1$ , by approaching the singularity as  $\delta$  varies from  $10^{-3}$  to  $10^{-6}$ . In particular, these properties explain why the topological charge determined by Eq. (4) changes at the critical resistivity  $\rho = 1$ , as the band gap closes when the branches touch at the divergence point.

Importantly, the band gap that separates the positive and negative frequency spectra [see Fig. 3(c)] closes for any value of the normalized resistivity in the range  $0.9434 < |\rho| < 0.9434^{-1}$  [see Figs. 3(d) and 3(e)]. In fact, it turns out that the  $n = 1$  bands,  $\omega_1^{(+)}$  and  $\omega_1^{(-)}$ , may intersect for  $\rho$  near the singularity. Depending on the value of  $|\rho|$ , the intersection may be an isolated point (Fig. 3(d)) or correspond to a line degeneracy over the imaginary frequency axis (Fig. 3(e)). In the former case, the intersection occurs for a in-plane momentum on the order of  $k \approx 1.36/a$ . It is relevant to note that the range of  $\rho$  for which the  $n = 1$  bands intersect is determined uniquely by the geometry of the problem, and is totally independent of the plate width  $a$ <sup>54</sup>.

Evidently, for  $0.9434 < |\rho| < 0.9434^{-1}$  the topological charge of the  $n = 1$  bands is undefined. This range of  $\rho$  links the gapped phases through an intermediate collection of exceptional points (EPs). For  $\rho$  slightly larger than 0.9434 there is an isolated EP which unfolds into a line for larger values of  $\rho$  and then collapses into an isolated EP again as  $\rho$  approaches  $0.9434^{-1}$ . At the EPs, the eigenvectors of the  $n = 1$  spinors coalesce as  $\Psi_{\mathbf{k},1}^\pm \parallel \Psi_{\mathbf{k},-1}^\pm$ .

The modal equation (3) is invariant under the transformation  $\rho \rightarrow \rho^{-1}$  when  $\rho \neq 0$ . This implies that the band structure remains the same under the transformation  $\rho \rightarrow \rho^{-1}$ , i.e.,  $\omega_n(k; \rho) = \omega_n(k; \rho^{-1})$ . Due to this

symmetry, the projected band structure near the singularity  $\rho = 1$  is to a good approximation only a function of  $|\delta|$ . Thus, the plots in Figs. 3(c), 3(d) and 3(e) can be readily extended to negative values of  $\delta$ . Furthermore, taking into account that  $\omega_n(-\rho) = \omega_n^*(\rho)$  it is clear that the topological phase transitions develop in similar way around the points  $\rho = \pm 1$  where energy is resonantly dissipated or absorbed.

The closing and reopening of the gap mediates the exchange of topological charge between the negative and positive frequency parts of the spectrum. At the phase transition, each and every band flips the sign of its spin Chern number as predicted by Eq.(4). The exchange of topological charge between negative and positive frequencies has been discussed previously for nonreciprocal Chern insulators<sup>59,60</sup>.

Figure 3(f) presents the detailed topological phase diagram of  $\mathcal{C}_n^+$ . Interestingly, for a fixed  $\rho$  the Chern numbers of the different bands alternate between  $+1$  and  $-1$ . This implies that, while the topology of the individual bands is well-defined, the topology of the band gap itself is not. For instance, the gap Chern number for the pseudospin “+” and for  $|\rho| \ll 1$  is determined by the series  $\mathcal{C}_{\text{gap}}^+ = -1 + 1 - 1 + \dots$ , which is non-convergent. The origin of the ill-defined topology is rooted in the particle-hole symmetry of photonic systems<sup>61</sup>. In principle, this problem may be fixed with a suitable dispersive model for the plates that ensures that in the  $\omega \rightarrow \infty$  limit their electromagnetic response approaches that of the vacuum, so modes with sufficiently large  $n$  have a trivial topological charge<sup>61</sup>. In the Supplementary Material 54, we show that in the dispersive case it is reasonable to assume that the topological phase transition is governed by the exchange of the topological charge of the  $n = 1$  bands.

Notably, a parity inversion  $P_I : (x, y, z) \rightarrow (-x, -y, -z)$  exchanges the positions of the top and bottom plates. Since the electric and magnetic fields are odd/even under a parity inversion, it also exchanges the spin of the modes and the Chern numbers transform as  $[\mathcal{C}_n^\pm]_{P_I} = \mathcal{C}_n^\mp = -\mathcal{C}_n^\pm$ . This result holds true for a completely arbitrary (e.g., dispersive and inhomogeneous)  $\mathcal{PD}$ -reciprocal waveguide. In particular, it justifies why for our geometry exchanging the position of the plates ( $\rho \rightarrow 1/\rho$ ) flips all the Chern number signs<sup>54</sup>. Moreover, it indicates that the modes identified in<sup>18,55</sup> that propagate at the boundary of a guide with PEC-PMC walls and the corresponding  $P_I$  transformed guide with PMC-PEC walls may be understood as topologically protected edge states.

The difference between the Chern numbers of a guide and its  $P_I$  transformed counterpart is always even, meaning there is an even number of protected unidirectional states at the interface. In our specific system, we expect two edge states per pseudospin. For a fixed pseudospin, the edge states can be visualized as waves attached either to the top or to the bottom plates<sup>62</sup>. While for conventional insulators, it is not possible to guarantee protection against back-scattering when  $\mathcal{C}^+ - [\mathcal{C}^+]_{P_I}$  is

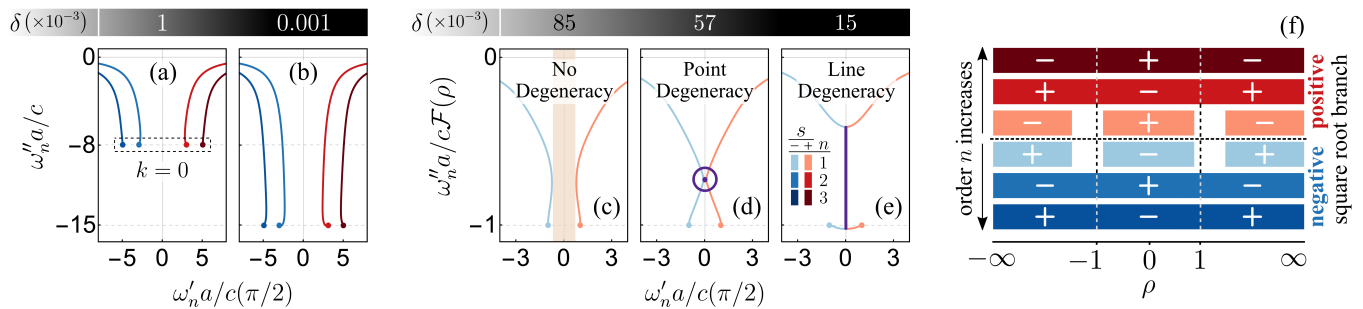


Figure 3: (a, b) Projected band structure in the complex plane for the first few higher-order bands  $\omega_n$  ( $n = 2, 3$ ) with  $\delta = 1 - |\rho| = 10^{-3}$  and  $\delta = 10^{-6}$ , respectively. The frequencies associated with  $k = 0$  are represented by the solid dots. (c, d, e) Illustration of the topological phase transition. The band gap between the positive and negative frequency branches with  $n = 1$  shown in (c) in beige closes at an isolated point  $k \approx 1.36/a$  when  $\delta$  reaches  $\delta \approx 57 \times 10^{-3}$ , as depicted in (d). In panel (e) the degeneracy widens to a line when the resistivity gets closer to the critical point  $\rho = 1$  ( $\delta = 15 \times 10^{-3}$ ). (f) Topological phase diagram for the PPW in Fig. 1. The spin Chern numbers  $C_n^\pm$  [Eq. (4)] are indicated for the range of  $\rho$  for which the band gap is open.

an even number, in the case of  $\mathcal{PD}$ -symmetric systems the protection against back-scattering is always guaranteed by the fact that the system Hamiltonian is a direct sum of the (uncoupled)  $\hat{\mathcal{H}}^\pm$  Hamiltonians.

In summary, we uncovered the topological properties of non-Hermitian  $\mathcal{PD}$ -symmetric and reciprocal photonic systems. We found that the Maxwell's equations can be split into two decoupled sets of spin-up and spin-down states, connected by the  $\mathcal{PD}$ -symmetry, even in non-Hermitian materials. By focusing on  $\mathcal{PD}$ -symmetric parallel-plate guides, we discovered a robust zero-frequency band gap that separates the positive and negative frequency parts of the spectrum.

Through the use of non-Hermitian topological band theory, we determined the spin Chern numbers of the individual bands and observed a phase transition near  $\rho = \pm 1$ , separating two distinct topological phases. At the transition, the positive and negative frequency spectra merge creating either isolated exceptional points or a

continuum of EPs in the form of a line segment.

Our findings reveal that the bulk topologies of these  $\mathcal{PD}$ -symmetric photonic structures are highly resilient to non-Hermitian effects and explain the presence of protected edge modes at the interfaces of different  $\mathcal{PD}$ -symmetric guides.

## Acknowledgments

This work is partially supported by the IET under the A F Harvey Engineering Research Prize, by the Simons Foundation under the award 733700 (Simons Collaboration in Mathematics and Physics, ‘‘Harnessing Universal Symmetry Concepts for Extreme Wave Phenomena’’), and by Fundaao para a Ciencia e a Tecnologia and Instituto de Telecomunicaoes under project UIDB/50008/2020.

- <sup>1</sup> L. Lu, J. D. Joannopoulos, and M. Soljaci, Nature Photonics **8**, 821 (2014), ISSN 17494893.
- <sup>2</sup> M. Kim, Z. Jacob, and J. Rho, Light: Science & Applications **9** (2020), URL <https://doi.org/10.1038/s41377-020-0331-y>.
- <sup>3</sup> F. D. M. Haldane and S. Raghu, Phys. Rev. Lett. **100**, 013904 (2008), URL <https://link.aps.org/doi/10.1103/PhysRevLett.100.013904>.
- <sup>4</sup> S. Raghu and F. D. M. Haldane, Phys. Rev. A **78**, 033834 (2008), URL <https://link.aps.org/doi/10.1103/PhysRevA.78.033834>.
- <sup>5</sup> C. L. Kane and E. J. Mele, Phys. Rev. Lett. **95**, 226801 (2005), URL <https://link.aps.org/doi/10.1103/PhysRevLett.95.226801>.
- <sup>6</sup> F. Liu and J. Li, Phys. Rev. Lett. **114**, 103902 (2015), URL <https://link.aps.org/doi/10.1103/PhysRevLett.114.103902>.
- <sup>7</sup> K. Y. Bliokh, D. Smirnova, and F. Nori, Science **348**,

- 1448 (2015), URL <https://doi.org/10.1126/science.aaa9519>.
- <sup>8</sup> M. C. Rechtsman, J. M. Zeuner, Y. Plotnik, Y. Lumer, D. Podolsky, F. Dreisow, S. Nolte, M. Segev, and A. Szameit, Nature **496**, 196 (2013), URL <https://doi.org/10.1038/nature12066>.
- <sup>9</sup> W. Gao, M. Lawrence, B. Yang, F. Liu, F. Fang, B. Beri, J. Li, and S. Zhang, Phys. Rev. Lett. **114**, 037402 (2015), URL <https://link.aps.org/doi/10.1103/PhysRevLett.114.037402>.
- <sup>10</sup> A. B. Khanikaev, S. H. Mousavi, W.-K. Tse, M. Kargarian, A. H. MacDonald, and G. Shvets, Nature Materials **12**, 233 (2012), URL <https://doi.org/10.1038/nmat3520>.
- <sup>11</sup> T. Ma, A. B. Khanikaev, S. H. Mousavi, and G. Shvets, Phys. Rev. Lett. **114**, 127401 (2015), URL <https://link.aps.org/doi/10.1103/PhysRevLett.114.127401>.
- <sup>12</sup> W.-J. Chen, S.-J. Jiang, X.-D. Chen, B. Zhu, L. Zhou, J.-W. Dong, and C. T. Chan, Nature Communications **5**

- (2014), URL <https://doi.org/10.1038/ncomms6782>.
- 13 A. Slobozhanyuk, S. H. Mousavi, X. Ni, D. Smirnova, Y. S. Kivshar, and A. B. Khanikaev, *Nature Photonics* **11**, 130 (2016), URL <https://doi.org/10.1038/nphoton.2016.253>.
  - 14 X. Cheng, C. Jouvaud, X. Ni, S. H. Mousavi, A. Z. Genack, and A. B. Khanikaev, *Nature Materials* **15**, 542 (2016), URL <https://doi.org/10.1038/nmat4573>.
  - 15 C. He, X.-C. Sun, X.-P. Liu, M.-H. Lu, Y. Chen, L. Feng, and Y.-F. Chen, *Proceedings of the National Academy of Sciences* **113**, 4924 (2016), URL <https://doi.org/10.1073/pnas.1525502113>.
  - 16 M. G. Silveirinha, *Phys. Rev. B* **93**, 075110 (2016), URL <https://link.aps.org/doi/10.1103/PhysRevB.93.075110>.
  - 17 M. G. Silveirinha, *Physical Review B* **95** (2017), URL <https://doi.org/10.1103/physrevb.95.035153>.
  - 18 W.-J. Chen, Z.-Q. Zhang, J.-W. Dong, and C. T. Chan, *Nature Communications* **6** (2015), URL <https://doi.org/10.1038/ncomms9183>.
  - 19 S. Lannebère and M. G. Silveirinha, *Nanophotonics* **8**, 1387 (2019), URL <https://doi.org/10.1515/nanoph-2019-0037>.
  - 20 M. G. Silveirinha, *Physical Review B* **99** (2019), URL <https://doi.org/10.1103/physrevb.99.125155>.
  - 21 H. Shen, B. Zhen, and L. Fu, *Physical Review Letters* **120** (2018), URL <https://doi.org/10.1103/physrevlett.120.146402>.
  - 22 Z. Yu, G. Veronis, Z. Wang, and S. Fan, *Phys. Rev. Lett.* **100**, 023902 (2008), URL <https://link.aps.org/doi/10.1103/PhysRevLett.100.023902>.
  - 23 Z. Wang, Y. Chong, J. D. Joannopoulos, and M. Soljačić, *Nature* **461**, 772 (2009), URL <https://doi.org/10.1038/nature08293>.
  - 24 Y. Poo, R.-x. Wu, Z. Lin, Y. Yang, and C. T. Chan, *Phys. Rev. Lett.* **106**, 093903 (2011), URL <https://link.aps.org/doi/10.1103/PhysRevLett.106.093903>.
  - 25 D. A. Jacobs, A. E. Miroshnichenko, Y. S. Kivshar, and A. B. Khanikaev, *New Journal of Physics* **17**, 125015 (2015), URL <https://doi.org/10.1088/1367-2630/17/12/125015>.
  - 26 R. Fleury, A. B. Khanikaev, and A. Alù, *Nature Communications* **7** (2016), URL <https://doi.org/10.1038/ncomms11744>.
  - 27 M. G. Silveirinha, *Phys. Rev. B* **94**, 205105 (2016), URL <https://link.aps.org/doi/10.1103/PhysRevB.94.205105>.
  - 28 B. Midya, H. Zhao, and L. Feng, *Nature Communications* **9** (2018), URL <https://doi.org/10.1038/s41467-018-05175-8>.
  - 29 C. Poli, M. Bellec, U. Kuhl, F. Mortessagne, and H. Schomerus, *Nature Communications* **6** (2015), URL <https://doi.org/10.1038/ncomms7710>.
  - 30 M. Pan, H. Zhao, P. Miao, S. Longhi, and L. Feng, *Nature Communications* **9** (2018), URL <https://doi.org/10.1038/s41467-018-03822-8>.
  - 31 C. Dembowski, H.-D. Gräf, H. L. Harney, A. Heine, W. D. Heiss, H. Rehfeld, and A. Richter, *Phys. Rev. Lett.* **86**, 787 (2001), URL <https://link.aps.org/doi/10.1103/PhysRevLett.86.787>.
  - 32 H. Xu, D. Mason, L. Jiang, and J. G. E. Harris, *Nature* **537**, 80 (2016), URL <https://doi.org/10.1038/nature18604>.
  - 33 D. Leykam, K. Y. Bliokh, C. Huang, Y. D. Chong, and F. Nori, *Phys. Rev. Lett.* **118**, 040401 (2017), URL <https://link.aps.org/doi/10.1103/PhysRevLett.118.040401>.
  - 34 K. Esaki, M. Sato, K. Hasebe, and M. Kohmoto, *Phys. Rev. B* **84**, 205128 (2011), URL <https://link.aps.org/doi/10.1103/PhysRevB.84.205128>.
  - 35 S.-D. Liang and G.-Y. Huang, *Phys. Rev. A* **87**, 012118 (2013), URL <https://link.aps.org/doi/10.1103/PhysRevA.87.012118>.
  - 36 T. E. Lee, *Phys. Rev. Lett.* **116**, 133903 (2016), URL <https://link.aps.org/doi/10.1103/PhysRevLett.116.133903>.
  - 37 H. Menke and M. M. Hirschmann, *Phys. Rev. B* **95**, 174506 (2017), URL <https://link.aps.org/doi/10.1103/PhysRevB.95.174506>.
  - 38 H. Zhou, C. Peng, Y. Yoon, C. W. Hsu, K. A. Nelson, L. Fu, J. D. Joannopoulos, M. Soljačić, and B. Zhen, *Science* **359**, 1009 (2018), URL <https://doi.org/10.1126/science.aap9859>.
  - 39 M.-A. Miri and A. Alù, *Science* **363** (2019), URL <https://doi.org/10.1126/science.aar7709>.
  - 40 M. Berry, *Czechoslovak Journal of Physics* **54**, 1039 (2004), URL <https://doi.org/10.1023/b:cjop.0000044002.05657.04>.
  - 41 M. V. Keldysh, *Russian Mathematical Surveys* **26**, 15 (1971), URL <https://doi.org/10.1070/rm1971v026n04abeh003985>.
  - 42 T. Kato, *Perturbation theory for linear operators*, vol. 132 (Springer Science & Business Media, 2013).
  - 43 N. Moiseyev, *Non-Hermitian quantum mechanics* (Cambridge University Press, 2011).
  - 44 R. Uzdin, A. Mailybaev, and N. Moiseyev, *Journal of Physics A: Mathematical and Theoretical* **44**, 435302 (2011), URL <https://doi.org/10.1088/1751-8113/44/43/435302>.
  - 45 M. Berry and R. Uzdin, *Journal of Physics A: Mathematical and Theoretical* **44**, 435303 (2011), ISSN 17518113, URL <http://search.ebscohost.com/login.aspx?direct=true&db=edselc&AN=edselc.2-52.0-80054076926&site=eds-live>.
  - 46 M. V. Berry, *Journal of Optics* **13**, 115701 (2011), URL <https://doi.org/10.1088/2040-8978/13/11/115701>.
  - 47 I. Gilary, A. A. Mailybaev, and N. Moiseyev, *Phys. Rev. A* **88**, 010102 (2013), URL <https://link.aps.org/doi/10.1103/PhysRevA.88.010102>.
  - 48 E.-M. Graefe, A. A. Mailybaev, and N. Moiseyev, *Phys. Rev. A* **88**, 033842 (2013), URL <https://link.aps.org/doi/10.1103/PhysRevA.88.033842>.
  - 49 T. J. Milburn, J. Doppler, C. A. Holmes, S. Portolan, S. Rotter, and P. Rabl, *Phys. Rev. A* **92**, 052124 (2015), URL <https://link.aps.org/doi/10.1103/PhysRevA.92.052124>.
  - 50 J. Doppler, A. A. Mailybaev, J. Böhm, U. Kuhl, A. Girschik, F. Libisch, T. J. Milburn, P. Rabl, N. Moiseyev, and S. Rotter, *Nature* **537**, 76 (2016), URL <https://doi.org/10.1038/nature18605>.
  - 51 D. E. Fernandes and M. G. Silveirinha, *Phys. Rev. Applied* **12**, 014021 (2019), URL <https://link.aps.org/doi/10.1103/PhysRevApplied.12.014021>.
  - 52 D. J. Bisharat and D. F. Sievenpiper, *Phys. Rev. Lett.* **119**, 106802 (2017), URL <https://link.aps.org/doi/10.1103/PhysRevLett.119.106802>.
  - 53 D. J. Bisharat and D. F. Sievenpiper, *Laser & Photonics Reviews* **13**, 1900126 (2019).
  - 54 Supplementary material with: (I) Symmetry-Induced De-

- coupling of Maxwell's Equations. (II) Boundary conditions in the PPW. (III) Bulk Modes. (IV) Spin Chern numbers for the pseudospin states. (V) Band structure near phase transition. (VI) Useful limits and symmetries.
- <sup>55</sup> E. Martini, M. G. Silveirinha, and S. Maci, *IEEE Transactions on Antennas and Propagation* **67**, 1035 (2019), URL <https://doi.org/10.1109/tap.2018.2880091>.
- <sup>56</sup> D. N. Sheng, Z. Y. Weng, L. Sheng, and F. D. M. Haldane, *Phys. Rev. Lett.* **97**, 036808 (2006), URL <https://link.aps.org/doi/10.1103/PhysRevLett.97.036808>.
- <sup>57</sup> J. A. Nelder and R. Mead, *The Computer Journal* **7**, 308 (1965), URL <https://doi.org/10.1093/comjnl/7.4.308>.
- <sup>58</sup> M. G. Silveirinha, *Physical Review B* **92** (2015), URL <https://doi.org/10.1103/physrevb.92.125153>.
- <sup>59</sup> D. Jin, L. Lu, Z. Wang, C. Fang, J. D. Joannopoulos, M. Soljačić, L. Fu, and N. X. Fang, *Nature Communications* **7** (2016), URL <https://doi.org/10.1038/ncomms13486>.
- <sup>60</sup> S. Lannebère and M. G. Silveirinha, *Phys. Rev. B* **97**, 165128 (2018).
- <sup>61</sup> F. R. Prudêncio and M. G. Silveirinha, *Phys. Rev. Lett.* **129**, 133903 (2022).
- <sup>62</sup> N. Mohammadi Estakhri, N. Engheta, and R. Kastner, *Phys. Rev. Lett.* **124**, 033901 (2020), URL <https://link.aps.org/doi/10.1103/PhysRevLett.124.033901>.